Seasonal variation of atmospheric elemental carbon aerosols at Zhongshan Station, East Antarctica

LIU Yan[1], LI Chuanjin[1*], WANG Xiaoming[1], DING Minghu[1,2], DU Zhiheng[1], SHI Guitao[3], SUN Bo[4], KANG Shichang[1] & XIAO Cunde[1,5]

[1] State Key Laboratory of Cryospheric Science, Northwest Institute of Eco-Environment and Resources, Chinese Academy of Sciences, Lanzhou 730000, China;

[2] Institute of Meteorological Sciences in Tibetan Plateau and Polar Regions, Chinese Academy of Meteorological Sciences, Beijing 100081, China;

[3] Key Laboratory of Geographic Information Science, Ministry of Education, School of Geographic Sciences and State Key Lab of Estuarine and Coastal Research, East China Normal University, Shanghai 200241, China;

[4] Key Laboratory for Polar Science, MNR, Polar Research Institute of China, Shanghai 200062, China;

[5] State Key Laboratory of Earth Surface Processes and Resource Ecology, Beijing Normal University, Beijing 100875, China

Abstract   Elemental carbon (or black carbon) (EC or BC) aerosols emitted by biomass burning and fossil fuel combustion could cause notable climate forcing. Southern Hemisphere biomass burning emissions have contributed substantially to EC deposition in Antarctica. Here, we present the seasonal variation of EC determined from aerosol samples acquired at Zhongshan Station (ZSS), East Antarctica. The concentration of EC in the atmosphere varied between 0.02 and 257.81 ng·m^{-3} with a mean value of 44.87±48.92 ng·m^{-3}. The concentration of EC aerosols reached its peak in winter (59.04 ng·m^{-3}) and was lowest (27.26 ng·m^{-3}) in summer. Back trajectory analysis showed that biomass burning in southern South America was the major source of the EC found at ZSS, although some of it was derived from southern Australia, especially during winter. The 2019–2020 Australian bush fires had some influence on EC deposition at ZSS, especially during 2019, but the contribution diminished in 2020, leaving southern South America as the dominant source of EC.

Keywords   Zhongshan Station, elemental carbon aerosols, seasonal variations

1   Introduction

Elemental carbon (EC) or black carbon (BC) is a floc that is granular or composed of particles, resulting from incomplete combustion of fossil fuels or biomass (Andreae and Crutzen, 1997; Ma et al., 2020; Marquetto et al., 2020a,

2020b; Li et al., 2022). Atmospheric EC has two main sources: natural sources and anthropogenic sources (Ming et al., 2006; Koch et al., 2007; Hara et al., 2008; Bond et al., 2013; Ma et al., 2020). Natural sources mainly include forest fires and volcanic eruptions (Ming et al., 2006), while anthropogenic sources mainly refer to emissions from incomplete burning of fossil fuels and biomass (Ming et al., 2006; Bisiaux et al., 2012a). EC aerosols in the atmosphere can cause notable climatic effects. On the one hand, EC can

---

effectively absorb infrared and visible solar radiation in the atmosphere that leads to heating of the air (Bisiaux et al., 2012a, 2012b; Bond et al., 2013; Kang et al., 2020; Ma et al., 2020). On the other hand, EC nucleated aerosols can effectively reflect solar radiation, thereby reducing the amount of solar radiation reaching the Earth's and causing a cooling effect (McConnell et al., 2007; Bond et al., 2013; Painter et al., 2013). Additionally, EC aerosols suspended in the atmosphere can also interact with clouds and affect the atmospheric energy balance (Bond et al., 2013; Kang et al., 2020). When EC is deposited on the surface of snow and ice, it will reduce the surface albedo and strengthen the absorption of solar radiation, leading to intensification of melting, which can impart positive feedback on the climate system (Kang et al., 2020). The Fifth Assessment Report of the Intergovernmental Panel on Climate Change stated that radiative forcing caused by EC is $+0.64$ W·m^{-2}, and it predicted that the radiative forcing of EC might increase to $+0.71$ W·m^{-2} in the future, of which that caused by fossil fuel combustion would be $+0.51$ W·m^{-2} and that caused by biomass fuel combustion would be $+0.2$ W·m^{-2} (IPCC, 2013). Bond et al. (2013) illustrated that EC causes global mean radiative forcing of $+1.1$ W·m^{-2}. Under the scenario of increasing global emissions, EC has become the second most important factor after carbon dioxide in terms of impact on atmospheric radiative forcing (Andreae and Crutzen, 1997; Jacobson, 2001; Qian et al., 2011; Skiles et al., 2012; Bond et al., 2013; Arienzo et al., 2017; Zhang and Kang, 2017).

Since the Industrial Revolution, increasing concentrations of EC have been detected in the cryosphere, with most related studies focused on the Arctic, Himalayas, and Europe because such regions are close to areas of human activity and are reasonably accessible (McConnell et al., 2007; Zennaro et al., 2014; Kang et al., 2020). Antarctica is far from other continents, without intensive human activities, and is aerially blocked by the westerly circulation that prevails throughout the year (Kakareka, 2020; Kakareka and Salivonchyk, 2020; Kakareka and Kukharchyk, 2022). Therefore, Antarctica is considered the last remaining pristine land on Earth (Zhang et al., 2015). Owing to its isolation, Antarctica is also considered the region that represents the background environmental EC (Chýlek et al., 1987, 1992; Warren and Clarke, 1990; Bisiaux et al., 2012a, 2012b; Ma et al., 2020). Therefore, EC is considered to have negligible impact on the snow–ice albedo and climatic system of Antarctica (Grenfell et al., 1994; Bisiaux et al., 2012a, 2012b; Khan et al., 2018; Ma et al., 2020). However, significant increase in EC deposition on the continent has been detected from thousands of years previously to recent decades (Bisiaux et al., 2012a; Li et al., 2022), and biomass burning and human activities on surrounding continents and countries (i.e., South America, Australia, New Zealand, and South Africa) have been considered as potential sources and influencing factors (Bisiaux et al., 2012a). Currently, controversy remains regarding the source regions of Antarctic EC aerosols and the primary pathways of transport. For example, Fiebig et al. (2009) suggested that central Brazil was the main source region of EC in East Antarctica, while Marquetto et al. (2020a) argued that the main contributor to modern western Antarctic EC was biomass combustion in Australia and New Zealand.

Few studies have examined the EC in East Antarctica, especially in regions facing the Indian Ocean sector of the Southern Ocean (Chaubey et al., 2010; Srivastava et al., 2021). Moreover, because previous work mainly used ice cores as the research medium, the relatively low temporal resolution made it difficult to study the detailed variation pattern (Bisiaux et al., 2012a, 2012b; Li et al., 2022). Here, we present the results of a five-year (February 2016 to December 2020) high temporal resolution (weekly) campaign of continuous monitoring of atmospheric EC aerosols in the coastal region of East Antarctica facing the Indian Ocean sector of the Southern Ocean. The objectives were to elucidate the seasonal variation of EC and to study the potential source regions, transport pathways, and related influencing mechanisms.

2   Materials and methods

2.1   Sampling

Since February 2016, a high-volume (1000 L·min^{-1}) total suspended particulate sampling instrument (Wuhan Tianhong Company, China) has been operating at Zhongshan Station (ZSS; 69°37′31″S, 76°22′14″E) (Figure 1) to monitor atmospheric environmental conditions (Li et al., 2020). ZSS is located in the coastal area of East Antarctica, facing the Indian Ocean sector of the Southern Ocean. According to monitoring results of meteorological conditions at ZSS during our sampling campaign (February 2016 to December 2020), the annual mean air temperature was −9.2℃, with the lowest recorded temperature of −45℃. The average annual number of precipitation days was 142, and almost all precipitation was in the form of snowfall. The wind speed was reasonably high, with winds above grade 8 (17.2–20.4 m·s^{-1}) occurring on up to 174 d annually, and the maximum recorded wind speed was 50.3 m·s^{-1}. To avoid potential contamination from the activities conducted at ZSS, the sampling site was established on bare rock at the northernmost point accessible, which is approximately 100 and 600 m from the ocean and the research station, respectively. The predominant easterly surface wind at the sampling site effectively minimizes the transport of air from the direction of ZSS (Li et al., 2020).

Sampling was normally conducted once per week. Before the field season, all the required Whatman 41 quartz filters (20 cm×25 cm; Whatman Ltd., Maidstone, UK) were wrapped in aluminum foil, placed in a muffle oven, and baked at 500℃ for 5 h to remove organic impurities (Li et al., 2020). After cooling to room temperature, the filters were placed in a box held at constant temperature (25±3℃)

and constant humidity (22%±3%) for 72 h. Field blank filters were collected by exposing filters in the sampler but without drawing air through them; these were acquired to account for any artifacts that might have been introduced during the sample handling process. Between February 2006 and December 2020, 230 filters were collected. After each

sampling, the filters were sealed with aluminum foil and stored in a cold and dark refrigerator. At the end of each field season, the filters were shipped back to the State Key Laboratory of Cryospheric Science (SKLCS) in Lanzhou (China) in frozen state (i.e., below −18℃) and stored in a dark refrigerator (−20℃) until required for further processing.
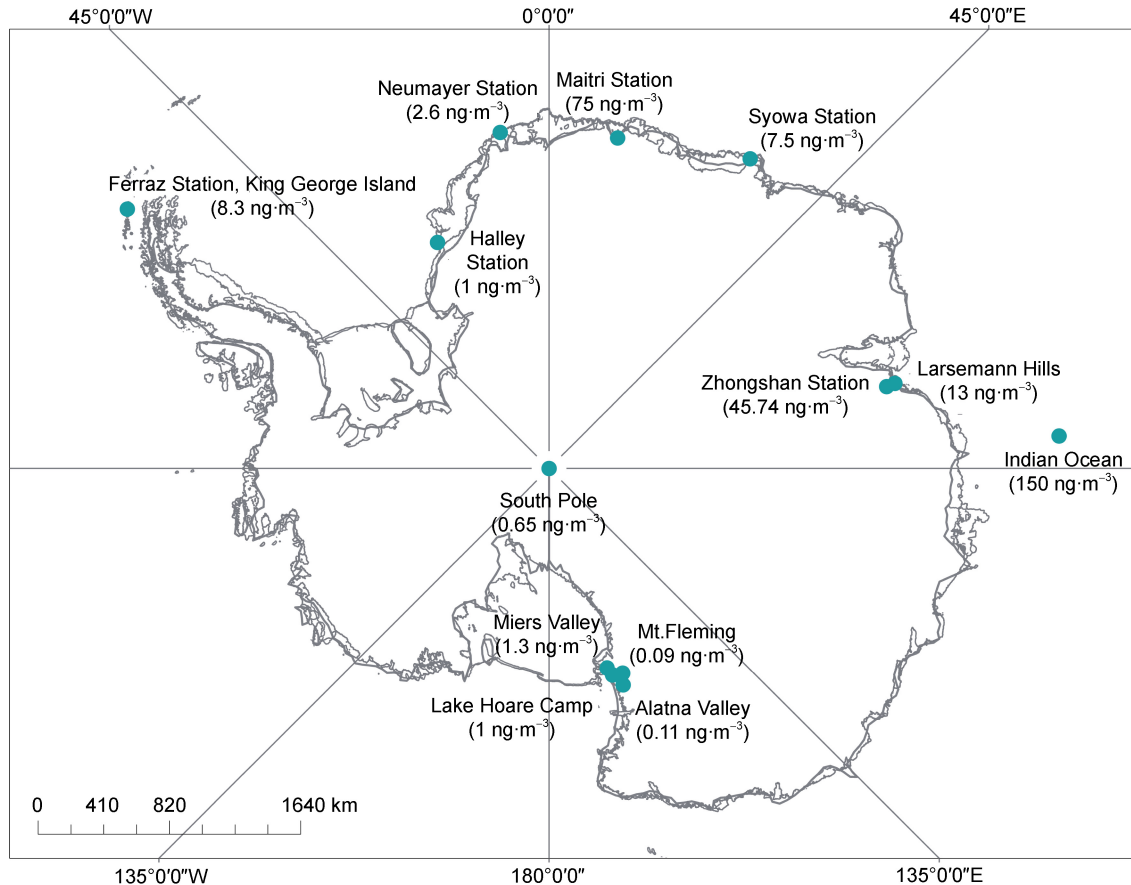
Figure 1 The location of the sampling site at Zhongshan Station (ZSS), and locations of atmospheric EC aerosol concentration measurements at other sites in Antarctica (Hansen et al., 1988; Bodhaine, 1995; Pereira et al., 2006; Hara et al., 2008; Chaubey et al., 2010; Weller et al., 2013; Khan et al., 2018; Srivastava et al., 2021).

Data of meteorological parameters (i.e., wind speed, wind direction, and days with strong winds) at ZSS were obtained from the Chinese Academy of Meteorological Sciences, and from automatic weather stations that performed measurements at 6-h intervals. For each parameter, 7308 measured data and 230 meteorological data samples (i.e., temperature and relative humidity) were acquired.

2.2   Sample analysis

2.2.1   EC analysis

An organic carbon (OC)/EC analyzer (Sunset Laboratory Inc., USA) was used to test for EC via thermal light reflection analysis at the SKLCS of the Northwest Institute of Eco-Environment and Resources, Chinese Academy of Sciences (Brown et al., 2019; Vodička et al., 2020). The

detected limit of EC is 0.02 $\mu g \cdot cm^{-2}$ (Brown et al., 2019). The program was set to Improve A, and the operating temperature range was between 1 and 840°C. The OC and EC were released by heating at different temperatures and detected by the flame ionization detector (Brown et al., 2019). Each sample was heated gradually in a nonoxidizing environment of He, causing OC to be heated and volatilized. Then, gradual heating continued in an He/O_2 environment (Brown et al., 2019). In the process, EC was oxidized to a gaseous oxide for quantitative detection, and then fed into quantitative He/CH_4 for calibration (Brown et al., 2019). During the entire process, a laser beam was shone on the quartz film, and the transmitted or reflected light gradually decreased when the OC carbonized. When the He was switched to He/O_2 and heated, the transmitted or reflected laser light gradually increased with the carbonization and oxidation decomposition of EC (Brown et al., 2019). The

initial intensity moment is called the OC/EC segmentation point; that is, the carbon detected before (after) this moment is defined as OC (EC).

2.2.2 Soluble ions analysis

Cations (i.e., Na^+, K^+, Mg^{2+}, Ca^{2+}, and NH_4^+) were analyzed using a Dionex 600 with an Ion Pac CS-12A 4 mm analytical column, CG-12A guard column, CSRS-ULTRA 4 mm suppressor, 20 mM methanesulfonic acid (MSA) eluent, and a cation electrolytically regenerated suppressor. Anions (Cl^-, NO_3^-, and SO_4^{2-}) were analyzed using a ICS-2500 ion chromatograph (ICS-2500, Thermo Scientific, USA) with an Ion Pac AS11-HC analytical column, AS11-HC guard column, ASRS-ULTRA II 4 mm suppressor, KOH eluent and an anion electrolytically regenerated suppressor. For all measured ions, the detection limit was 1 ng·g^{-1}; that is, three times the standard deviation of the noise from the baseline. The limit of quantification, defined as 10 times the standard deviation, was 3 ng·g^{-1}. Blanks were monitored regularly during sample analysis, and all blanks were found to be lower than the detection limit. All tests were completed in the Ultra-Clean Laboratory of the SKLCS of the Northwest Institute of Eco-Environment and Resources, Chinese Academy of Sciences.

Thorough pretreatment was necessary before the ion tests were conducted. First, three pieces of aerosol film with area of 2.83 cm^2 were adopted by a sampler, placed into a wide-mouth bottle with 20 mL of ultra-clean water for more than 60 min with an ultrasonic device, removed and filtered, and then tested on the machine. Finally, the concentration in the atmosphere is inferred from the ion concentration. The inference formula is expressed as: $y = pvs/s_1$, where p is the concentration of the measured ions, v is the volume of the prepared solution, s is the total aerosol film area placed in the field, and s_1 is the aerosol film area obtained with a sampler. The standard solution of the National Reference Standards Center, China was used to prepare the test standard, and the sample test results need blank correction and method correction.

In this study, Origin 2018, IBM SPSS Statistics 21,

Adobe Photoshop CC 2017, and Adobe Illustrator 2020 were used to process and analyze the content of BC, and the MeteoInfo backward trajectory model was used to analyze the source of the BC aerosols. Two forms of trajectory simulation are possible with the MeteoInfo model: backward transmission and forward diffusion. The former is mainly used to explain the problem of sinks, and the latter is mainly used to explain the problem of sources. The MeteoInfo model was used to track the backward trajectories from the coast of East Antarctica, and the clustering algorithm was used to group the trajectories according to the principle of closest trajectories, thereby representing the main sources of the air masses in the study area during the analysis period.

3 Results and discussion

3.1 Seasonal variation of EC and influencing factors

The mean concentration of atmospheric EC at ZSS during the sampling period (February 2016 to December 2020) was 44.87 ± 48.92 ng·m^{-3}, with a range of variation of 0.02–257.81 ng·m^{-3} (Figure 2). In comparison with other sites located in Antarctica and surrounding areas, the concentration at ZSS was always much higher than that inland and at some other coastal sites (Figure 1). However, EC at ZSS showed values comparable to those at Syowa Station and Maitri Station in East Antarctica (Hara et al., 2008; Chaubey et al., 2010), but much lower than those in the Indian and Atlantic sectors of the Southern Ocean surrounding the East Antarctica continent, which were even hundreds of times higher (Srivastava et al., 2021). The Antarctic continent, especially the interior region, is considered the last remaining pristine region on Earth, and the atmospheric EC concentrations are generally regarded as natural background values (Bisiaux et al., 2012a, 2012b). Previous measurements showed a gradient of increase in atmospheric EC concentrations from inland regions of Antarctica toward the coast, with the lowest EC concentration detected at the South Pole (i.e., 0.65 ng·m^{-3}), higher values near the eastern and western coasts
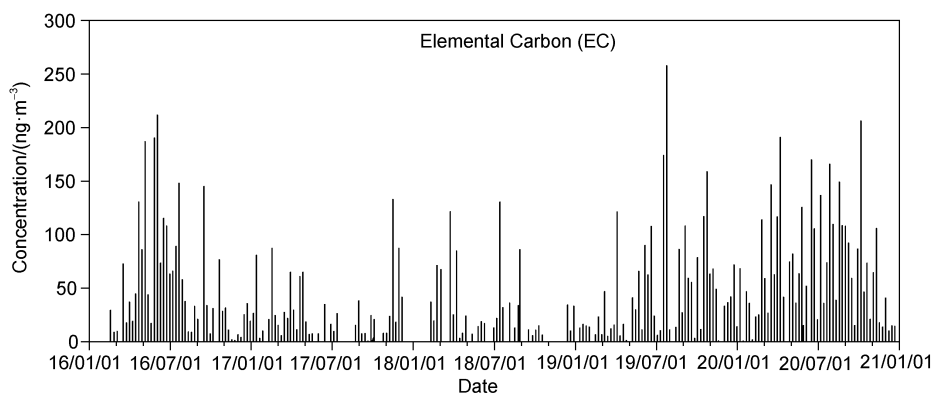

Figure 2   Temporal variation of atmospheric EC aerosols at ZSS during 2016–2020.

(2.6 ng·m^{-3}) (Bodhaine, 1995; Weller et al., 2013), and much higher concentrations on the Antarctic Peninsula (8.3 ng·m^{-3}) (Pereira et al., 2006). According to Hara et al. (2008), different transport mechanisms and variation in temporal distribution account for the discrepancy in EC concentration between different sites. Long-range transport via the lower troposphere during frequent storm conditions can lead to many peaks in atmospheric EC concentration over coastal Antarctica during the austral winter–spring seasons, whereas conditions favorable for EC transport via the free troposphere toward inland regions of Antarctica usually dominate during summer.

Statistical results show that atmospheric EC concentrations at ZSS always present the highest values during austral winter (June–August; $59.04\pm59.46 \text{ ng·m}^{-3}$), followed in descending order by those in austral autumn (March–May; $45.80\pm49.54 \text{ ng·m}^{-3}$), austral spring (September–November; $43.53\pm47.05 \text{ ng·m}^{-3}$), and austral summer (December–February; $27.26\pm25.81 \text{ ng·m}^{-3}$) (Figure 3). Notably, individual years and consecutive years show different variations, such as the low concentration of EC in winter 2017. This might reflect the impact of the westerly circulation restricting the contribution from South America (Figure S1). The entire pattern of seasonal variation is consistent with the EC deposited in snow layers near ZSS in East Antarctica (Ma et al., 2020). Ma et al. (2020) identified that the seasonal variation of EC is caused by EC emissions from source regions where bush fires and anthropogenic emissions of EC are intensified during winter and diminished during summer. However, because of the low temporal resolution of ice core records, no further detail on the variation could be extracted for comparison with our results. Monthly statistical results on the EC in aerosols at

ZSS show that the annual variation of EC has a single peak that occurs in July (Figure 4). This peak is 1 month earlier than that observed at Syowa Station (August) (Hara et al., 2008) and 3 months earlier than that observed at Neumayer, Halley, and Ferraz Stations (October) (Pereira et al., 2006; Weller et al., 2013). The observed difference prompted us to speculate that some factors other than emission source might also play an important role in influencing the seasonal variation of EC at ZSS. Hara et al. (2008) highlighted that the transport of EC via blizzards has considerable influence on its atmospheric concentration at coastal sites in East Antarctica, and that the higher concentrations observed during winter are always associated with strengthened katabatic winds that carry high concentrations of EC in continental air toward the coastal regions. The time of occurrence of high concentrations of EC during winter at ZSS is temporally consistent with the duration of strong winds. Meanwhile, the wind direction during winter always has a continental contribution (Figure 4). At ZSS, monthly statistical results show that July always has the highest number of days with strong winds (i.e., $>10 \text{ m·s}^{-1}$, weekly geometric mean value) and the greatest number of blizzards (Wang et al., 2011). However, this seems inconsistent with the statistical results of the meteorological conditions during our sampling campaign, which showed that the highest wind speeds and the highest number of days with strong winds occurred in August. We thus speculated that the actual concentrations of EC in continental air might play the dominant role, and that the difference in the wind direction in different months might also be partially responsible for that.

Correlation analysis (IBM SPSS Statistics, Version 21) was performed on the EC and major ions (Na^+, Cl^-, K^+,
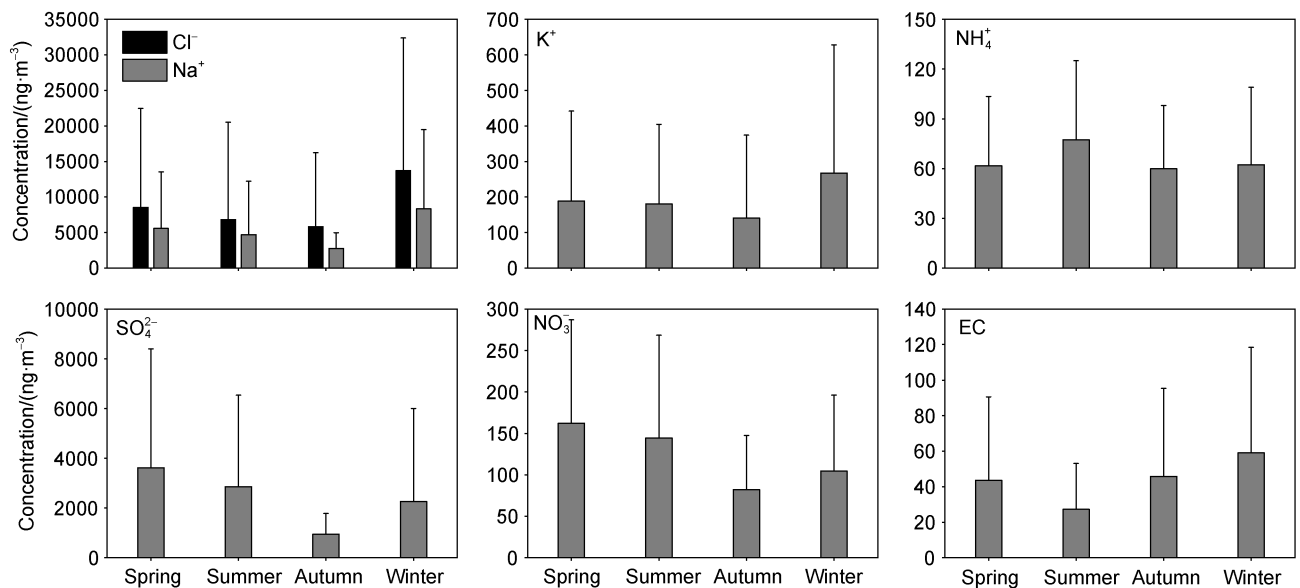
Figure 3 Seasonal variation of EC and other ions in atmospheric aerosols at ZSS during 2016–2020. Note: all data are expressed as the arithmetic means ± the standard deviation.
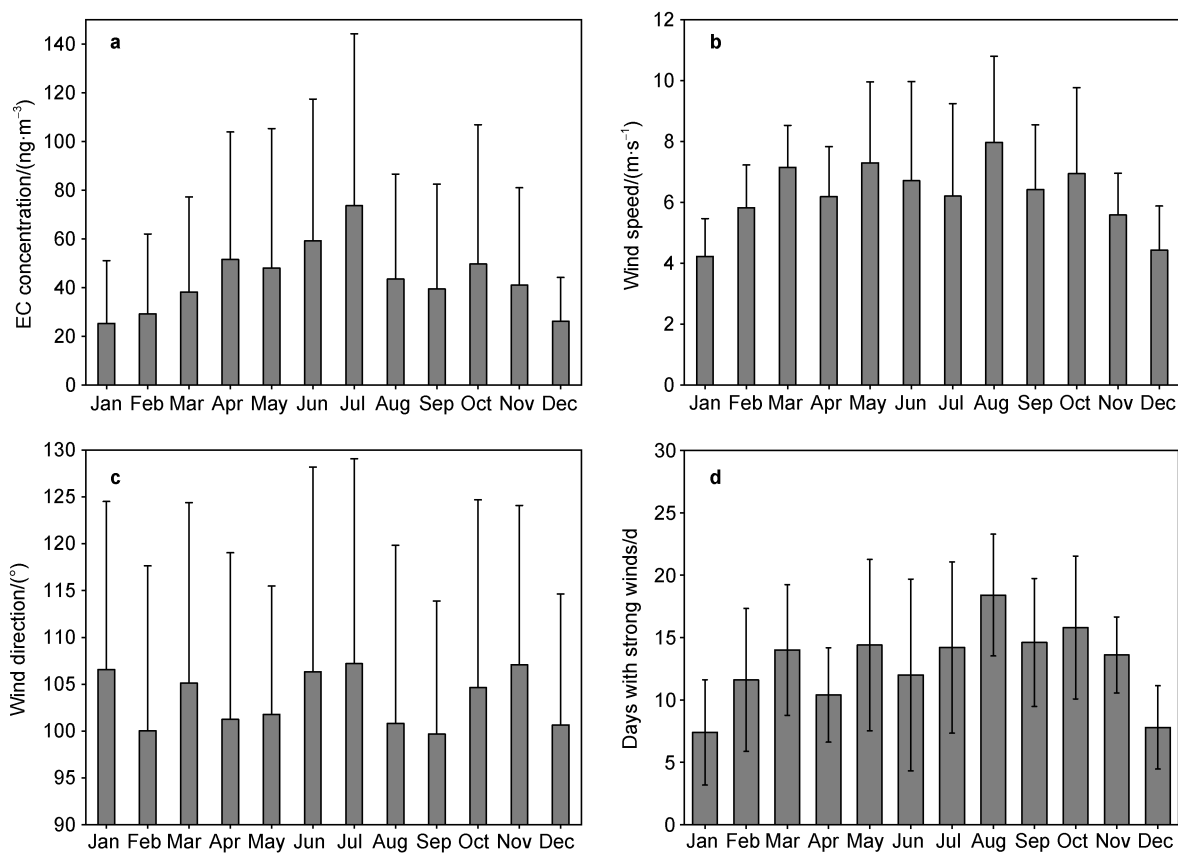
Figure 4　Monthly statistics of EC concentrations (**a**) in aerosols at ZSS, and monthly statistical results (**b**, **c**, **d**) of meteorological conditions (days per month with strong winds).

SO_4^{2-}, NO_3^-, Mg^{2+}, Ca^{2+}, and NH_4^+) of the aerosols, and the meteorological conditions (temperature, relative humidity, wind speed, and wind direction) (Table 1). Significant correlation was found between Na^+ and Cl^- and undoubtedly sea salt played the dominant role in their

deposition. No significant correlation was detected between EC and the ions of marine origin, implying that EC has different sources and transport pathways than the latter. However, EC and wind direction had positive correlation (R =0.229, $P<0.01$, n=230), which might indicate that material

Table 1　Correlation matrix between measured BC, ions, and meteorological parameters at ZSS derived via principal component analysis

	Cl^-	SO_4^{2-}	NO_3^-	Na^+	Mg^{2+}	Ca^{2+}	NH_4^+	EC	TEM	RH	WS	WD
Cl^-	1	0.319**	−0.086	0.859**	0.739**	0.331**	0.237**	−0.042	0.028	0.196**	0.467**	−0.164*
SO_4^{2-}		1	0.341**	0.384**	0.357**	0.535**	−0.027	0.054	0.172**	0.182**	0.085	−0.012
NO_3^-			1	−0.055	−0.004	0.128	−0.026	0.165*	0.138*	0.004	−0.223**	0.066
Na^+				1	0.594**	0.347**	0.140*	−0.047	0.069	0.175**	0.422**	−0.193**
Mg^{2+}					1	0.438**	0.139*	−0.018	0.008	0.223**	0.458**	−0.118
Ca^{2+}						1	−0.068	0.023	0.024	0.134*	0.123	−0.073
NH_4^+							1	−0.161*	0.094	0.127	0.147*	−0.035
EC								1	−0.290**	0.225**	−0.264**	0.229**
TEM									1	−0.036	0.021	−0.266**
RH										1	−0.108	0.075
WS											1	−0.395**
WD												1

Notes: TEM=Temperature, RH=Relative humidity, WS=Wind speed, WD=Wind direction. Different confidence levels are indicated as follows: ** for $P<0.01$, * for $P<0.05$, n=230

transported from the continental interior might carry more EC aerosols to the coastal regions. The positive correlation with relative humidity ($R=0.225$, $P<0.01$, $n=230$) indicates that relative humidity has some influence on the stagnation of the EC aerosols in the atmosphere.

3.2 Analysis of potential source regions

Controversy remains regarding the source regions of the EC found on the Antarctic continent (Bisiaux et al., 2012a, 2012b; Li et al., 2022). South America, Australia, and New Zealand have long been regarded as potential source regions for the EC deposited in Antarctica, especially West Antarctica, because forest fires, bush fires, and anthropogenic emissions usually contribute substantially to EC emissions within the Southern Hemisphere (Marquetto et al., 2020a, 2020b). Although southern Africa produces the largest emissions of EC annually in the Southern Hemisphere, it is considered a negligible source region for the EC deposited in Antarctica because of its relatively distant location and the blocking effect of the prevailing

westerly winds around Antarctica (Bisiaux et al., 2012a, 2012b).

To ascertain the potential source regions of the EC transported to ZSS, back trajectory analysis was conducted to track the pathways of the transporting air masses. For this purpose, the MeteoInfo model analysis method developed by the Chinese Academy of Meteorological Sciences for GIS applications and scientific computing environments was used in this study. Considering the maximum lifetime of EC in the troposphere (Bond et al., 2013; IPCC, 2013), we calculated the 14-d back trajectories during 2016–2020 from an initial height of 1000 m. All back trajectory calculations were driven using the National Centers for Environmental Prediction–National Center for Atmospheric Research (NCEP/NCAR) reanalysis data ($1°\times1°$, 17 vertical levels). We calculated the back trajectories of air masses in spring, summer, autumn, and winter, and the simulations for each season were grouped into clusters (Figure 5) using the model's cluster analysis algorithm. Meteorological track calculations were performed at 6-h intervals during the
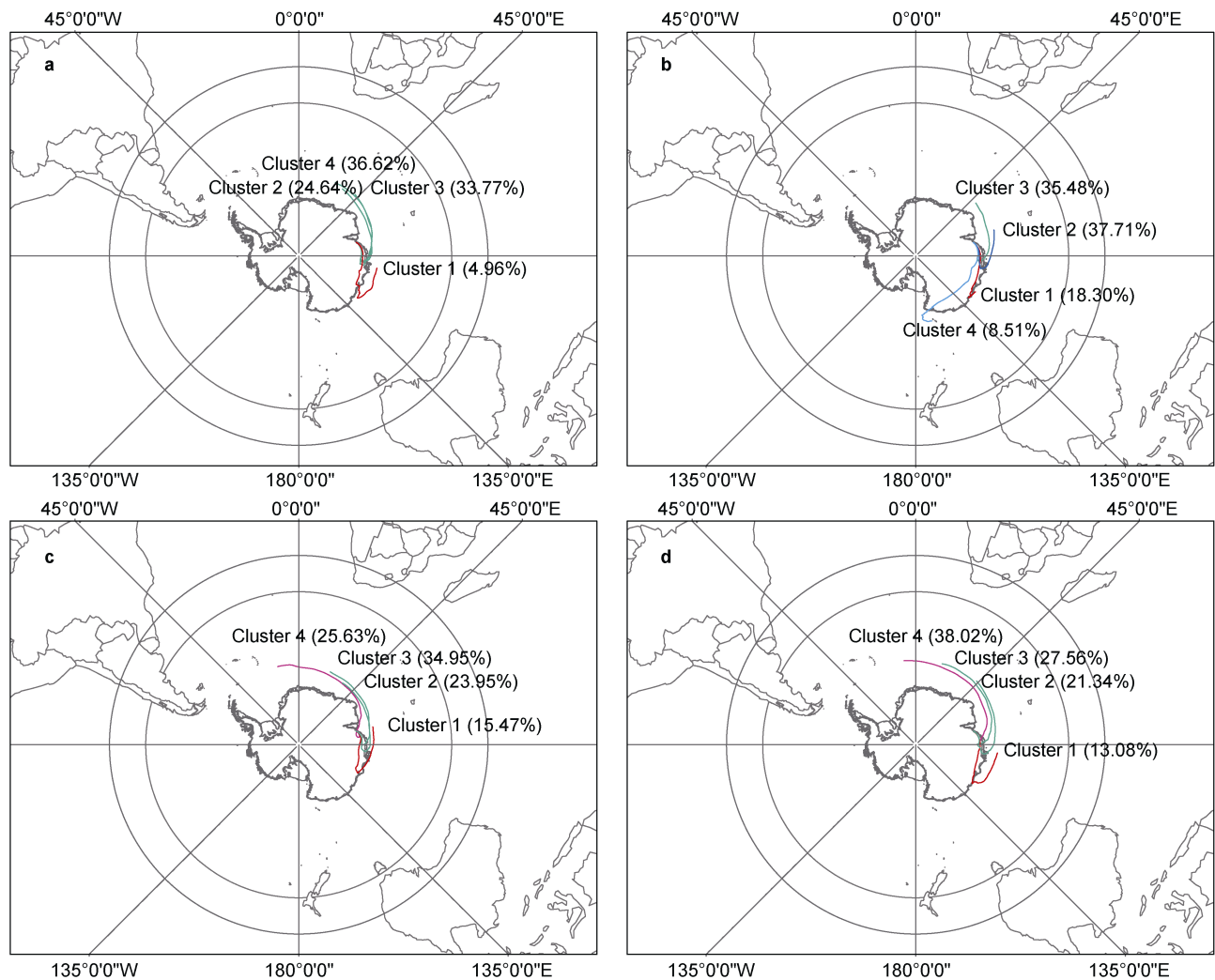
Figure 5 Backward trajectory clustering analysis of 14 d in four seasons at ZSS during 2016–2020: spring (**a**), summer (**b**), autumn (**c**), and winter (**d**) in the Southern Hemisphere, respectively. The date range of the analyzed day was the first to last day of the month.

entire calculation process. The analysis revealed that the movement of air masses in the four seasons was disturbed by the westerly wind, and that the air masses arriving at ZSS were mainly from the northwest; therefore, the westerly wind can be inferred to have important influence on the transport of atmospheric aerosols to the Antarctic continent. The westerly belt can transport EC to the troposphere, which then participates in the large-scale atmospheric circulation (Shi et al., 2019; Ma et al., 2020). Thus, BC emissions from Australia and South America could be transported via the atmospheric circulation to the coast of East Antarctica (Ma et al., 2020).

In comparison with other seasons, the long-range transport pathways of fast-moving air masses showed higher percentages during winter (38.02% for cluster 4; Figure 5d) and autumn (25.63% for cluster 4; Figure 5c), and their pathways were located closer to the air mass output pathway from southern South America, which might indicate higher loading of the air mass from southern South

America during autumn and winter. Spring and summer showed lower percentages of long-range transport pathways of the air masses, and the pathways were located further from the source region of South America. Most of the simulated air masses arriving at ZSS during spring and summer were characterized by clusters with slow speed, thereby indicating that local sources might play the major role in atmospheric input. Detailed trajectory information of all clusters also indicated certain influence from southern South America during all four seasons, together with possible influence from southern Australian sources, especially during winter (Figure 6).

3.3   Influences of the 2019–2020 Australian bush fires

An unusually strong positive Indian Ocean Dipole caused hot and dry weather in southeastern Australia in 2019, and devastating wildfires were promoted from June 2019 to December 2020 (Chang et al., 2021; Wang et al., 2022).
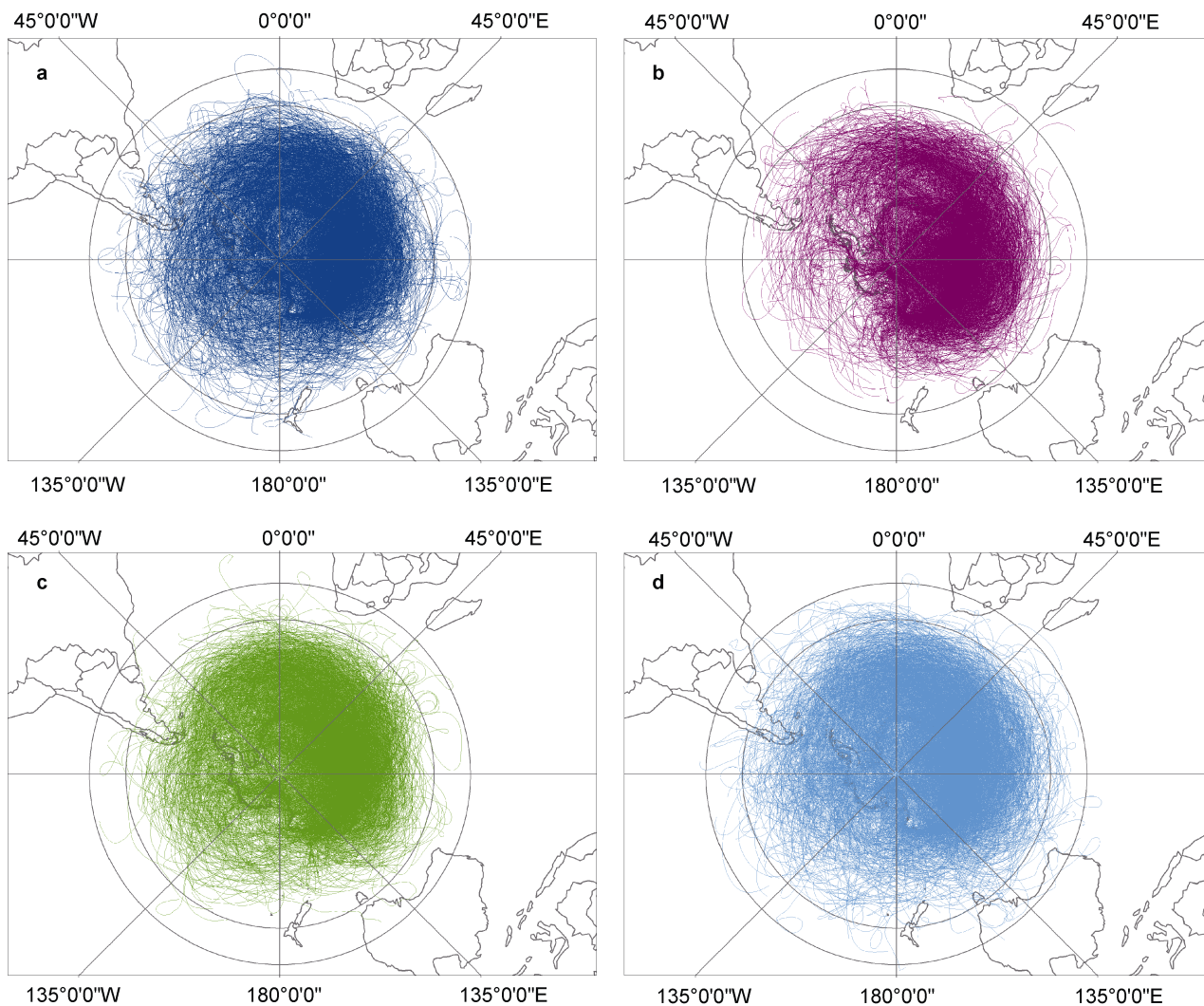

Figure 6   Plots for every cluster in the four seasons at ZSS from 2016 to 2020: spring (**a**), summer (**b**), autumn (**c**), and winter (**d**) in the Southern Hemisphere, respectively.

These extensive and severe wildfires started in June 2019 in Queensland and then extended to New South Wales and Victoria in eastern Australia. The most severe fires that developed in New South Wales and Victoria persisted from September 2019 to December 2020 (Filkov et al., 2020; Graham et al., 2021; Wang et al., 2022). The catastrophic and unprecedented 2019–2020 Australian bushfire season destroyed more than 3000 homes, killed at least 33 people, and earned it the epithet of the "Black Summer" (Filkov et al., 2020; Graham et al., 2021).

To investigate the potential influence of the 2019–2020 Australia bushfires on EC deposition at ZSS, we collected

details of the burned area in Australia from https://www.geo.vu.nl/~gwef/gfed/gfed4/. Furthermore, details of the burned area in southern South America were also collected, as shown in Figure 7. Annual mean EC concentration at ZSS showed significant increase in 2019, consistent with the simultaneous increase in the burned area in both Australia and southern South America (Figure 7). The burned area in Australia decreased in 2020, whereas a trend of increase was sustained in southern South America. The simultaneous increase in EC deposition at ZSS might indicate that emissions from the latter source provided the dominant contribution.
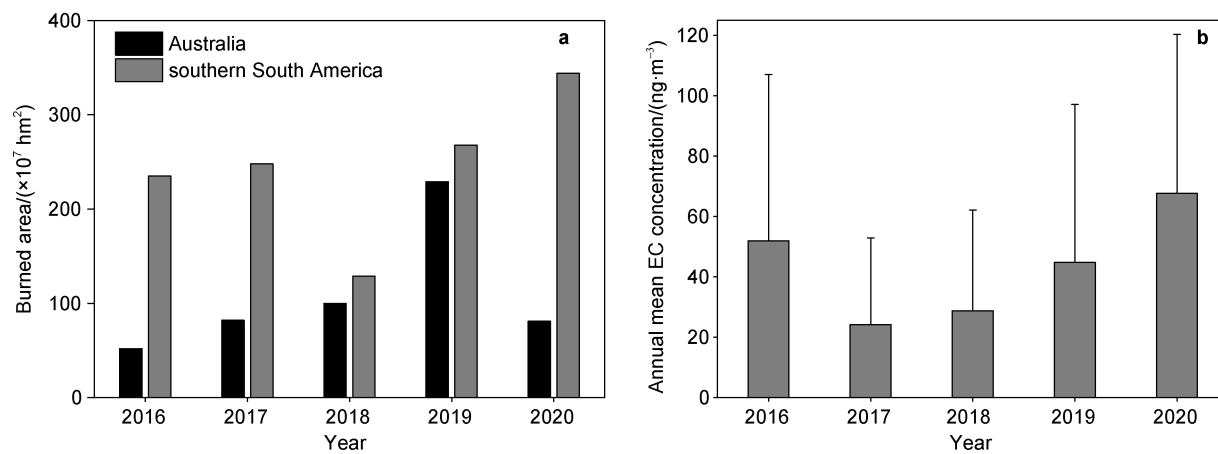
Figure 7 Monthly variation of burned area (**a**) in Australia and southern South America in relation with annual mean EC concentration at ZSS (**b**) from January 2019 to December 2020.

Monthly mean burned area data show that the highest values in Australia occurred during November–December 2019, whereas the highest values in southern South America in 2019 occurred in August–October; even higher values were detected during August–October 2020 in southern South America. From this, we speculate that southern South America might be the dominant source regions of the EC detected at ZSS. This is confirmed by the back trajectory results that indicate that southern South America might be the primary source region. However, some trajectories also extended to the southern part of Australia during winter; therefore, we cannot eliminate the potential for influence from Australian sources. Moreover, during the wildfires in 2019, an enormous volume of biomass-burning aerosols emitted from Australia traveled across the Pacific Ocean to reach South America (Chang et al., 2021).

4 Conclusions

This study analyzed the seasonal variation in the EC of atmospheric aerosols deposited during 2016–2020 at ZSS in East Antarctica. No significant correlation with the major ions was detected, implying that EC had different sources and different transport pathways. Higher EC concentrations were detected in winter, which coincided with higher emissions of EC from source regions in the Southern

Hemisphere, and periods of strong winds at ZSS. We speculated that air masses enriched with aerosols of EC transported from inland regions of Antarctica via katabatic winds made important contributions. Back trajectory analysis showed that southern South America was the major source region of the EC deposited at ZSS, although emissions from southern Australia also contributed, especially in winter. The 2019–2020 Australian bush fires also influenced EC deposition at ZSS, especially during 2019, but the contribution was diminished in 2020, leaving southern South America as the dominant source of EC.

References

Andreae M O, Crutzen P J. 1997. Atmospheric aerosols: biogeochemical sources and role in atmospheric chemistry. Science, 276(5315): 1052-1058, doi:10.1126/science.276.5315.1052.

Arienzo M M, McConnell J R, Murphy L N, et al. 2017. Holocene black carbon in Antarctica paralleled Southern Hemisphere climate. J Geophys Res Atmos, 122(13): 6713-6728, doi:10.1002/2017jd026599.

Bisiaux M M, Edwards R, McConnell J R, et al. 2012a. Changes in black carbon deposition to Antarctica from two high-resolution ice core records, 1850–2000 AD. Atmos Chem Phys, 12(9): 4107-4115, doi:10.5194/acp-12-4107-2012.

Bisiaux M M, Edwards R, McConnell J R, et al. 2012b. Variability of black carbon deposition to the East Antarctic Plateau, 1800–2000 AD. Atmos Chem Phys, 12(8): 3799-3808, doi:10.5194/acp-12-3799-2012.

Bodhaine B A. 1995. Aerosol absorption measurements at Barrow, Mauna Loa and the south pole. J Geophys Res Atmos, 100(D5): 8967, doi:10.1029/95jd00513.

Bond T C, Doherty S J, Fahey D W, et al. 2013. Bounding the role of black carbon in the climate system: a scientific assessment. J Geophys Res Atmos, 118(11): 5380-5552, doi:10.1002/jgrd.50171.

Brown S, Minor H, O'Brien T, et al. 2019. Review of sunset OC/EC instrument measurements during the EPA's sunset carbon evaluation project. Atmosphere, 10(5): 287, doi:10.3390/atmos10050287.

Chang D Y, Yoon J, Lelieveld J, et al. 2021. Direct radiative forcing of biomass burning aerosols from the extensive Australian wildfires in 2019–2020. Environ Res Lett, 16(4): 044041, doi:10.1088/1748-9326/abecfe.

Chaubey J P, Moorthy K K, Babu S S, et al. 2010. Black carbon aerosols over coastal Antarctica and its scavenging by snow during the Southern Hemispheric summer. J Geophys Res Atmos, 115(D10): D10210, doi:10.1029/2009jd013381.

Chýlek P, Srivastava V, Cahenzli L, et al. 1987. Aerosol and graphitic carbon content of snow. J Geophys Res Atmos, 92(D8): 9801-9809, doi:10.1029/jd092id08p09801.

Chýlek P, Johnson B, Wu H, et al. 1992. Black carbon concentration in Byrd Station ice core:from 13,000 to 700 years before present. Annales Geophysicae, 10(8): 625-629.

Fiebig M, Lunder C R, Stohl A. 2009. Tracing biomass burning aerosol from South America to Troll Research Station, Antarctica. Geophys Res Lett, 36(14): 171-183, doi:10.1029/2009gl038531.

Filkov A I, Ngo T , Matthews S, et al. 2020. Impact of Australia's catastrophic 2019/20 bushfire season on communities and environment. Retrospective analysis and current trends. J Saf Sci Resil, 1(1): 44-56, doi:10.1016/j.jnlssr.2020.06.009.

Graham A M, Pringle K J, Pope R J, et al. 2021. Impact of the 2019/2020 Australian megafires on air quality and health. GeoHealth, 5(10): e2021GH000454, doi: 10.1029/2021GH000454.

Grenfell T C, Warren S G, Mullen P C. 1994. Reflection of solar radiation by the Antarctic snow surface at ultraviolet, visible, and near-infrared wavelengths. J Geophys Res Atmos, 99(D9): 18669-18684, doi:10.1029/94jd01484.

Hansen A D A, Bodhaine B A, Dutton E G, et al. 1988. Aerosol black carbon measurements at the South Pole: initial results, 1986–1987. Geophys Res Lett, 15(11): 1193-1196, doi:10.1029/gl015i011p01193.

Hara K, Osada K, Yabuki M, et al. 2008. Measurement of black carbon at Syowa Station, Antarctica: seasonal variation, transport processes and pathways. Atmos Chem Phys Discuss, 8(3): 9883-9929.

IPCC. 2013. Climate change 2013: the physical science basis. Contribution of Working Group I to the fifth assessment report of the Intergovernmental Panel on Climate Change.

Jacobson M Z. 2001. Strong radiative heating due to the mixing state of black carbon in atmospheric aerosols. Nature, 409(6821): 695-697, doi:10.1038/35055518.

Kakareka S. 2020. Air pollutants and greenhouse gases emission inventory for power plants in the Antarctic. Adv Polar Sci, 31(4): 274-283, doi: 10.13679/j.advps.2020.0032.

Kakareka S, Kukharchyk T. 2022. Inventory of unintentional POPs emission from anthropogenic sources in Antarctica. Adv Polar Sci, 33(2): 156-166, doi:10.13679/j.advps.2021.0044.

Kakareka S, Salivonchyk S. 2020. An assessment of the impacts of diesel power plants on air quality in Antarctica. Adv Polar Sci, 31(1): 74-87, doi:10.13679/j.advps.2019.0029.

Kang S C, Zhang Y L, Qian Y, et al. 2020. A review of black carbon in snow and ice and its impact on the cryosphere. Earth Sci Rev, 210: 103346, doi:10.1016/j.earscirev.2020.103346.

Khan A L, McMeeking G R, Schwarz J P, et al. 2018. Near-surface refractory black carbon observations in the atmosphere and snow in the McMurdo Dry Valleys, Antarctica, and potential impacts of foehn winds. J Geophys Res Atmos, 123(5): 2877-2887, doi:10.1002/2017jd027696.

Koch D, Bond T C, Streets D, et al. 2007. Global impacts of aerosols from particular source regions and sectors. J Geophys Res Atmos, 112(D2): D02205, doi:10.1029/2005jd007024.

Li C J, Chen J B, Angot H, et al. 2020. Seasonal variation of mercury and its isotopes in atmospheric particles at the coastal Zhongshan Station, eastern Antarctica. Environ Sci Technol, 54(18): 11344-11355, doi:10.1021/acs.est.0c04462.

Li C J, Ma X Y, Dowdy A, et al. 2022. Changes in refractory black carbon (rBC) deposition to coastal eastern Antarctica during the past century. Glob Biogeochem Cycles, 36(8): e2021GB007223, doi:10.1029/2021gb007223.

Ma X Y, Li C J, Du Z H, et al. 2020. Spatial and temporal variations of refractory black carbon along the transect from Zhongshan Station to Dome A, eastern Antarctica. Atmos Environ, 242: 117816, doi:10.1016/j.atmosenv.2020.117816.

Marquetto L, Kaspari S, Simões J C. 2020a. Refractory black carbon (rBC) variability in a 47-year West Antarctic snow and firn core. Cryosphere, 14(5): 1537-1554, doi:10.5194/tc-14-1537-2020.

Marquetto L, Kaspari S, Simões J C, et al. 2020b. Refractory black carbon results and a method comparison between solid-state cutting and continuous melting sampling of a west Antarctic snow and firn core. Adv Atmos Sci, 37(5): 545-554, doi:10.1007/s00376-019-9124-8.

McConnell J R, Edwards R, Kok G L, et al. 2007. 20th-century industrial black carbon emissions altered Arctic climate forcing. Science, 317(5843): 1381-1384, doi:10.1126/science.1144856.

Ming J, Xiao C, Qin D. 2006. Climate forcing of black carbon in snow and ice. Adv Clim Change Res, 2(5): 238-241.

Painter T H, Seidel F C, Bryant A C, et al. 2013. Imaging spectroscopy of albedo and radiative forcing by light-absorbing impurities in mountain snow. J Geophys Res Atmos, 118(17): 9511-9523, doi:10.1002/jgrd. 50520.

Pereira E B, Evangelista H, Pereira K C D, et al. 2006. Apportionment of black carbon in the South Shetland Islands, Antarctic Peninsula. J

Geophys Res Atmos, 111(D3): D03303, doi:10.1029/2005jd006086.

Qian Y, Flanner M G, Leung L R, et al. 2011. Sensitivity studies on the impacts of Tibetan Plateau snowpack pollution on the Asian hydrological cycle and monsoon climate. Atmos Chem Phys, 11: 1929-1948, doi:10.5194/ACP-11-1929-2011.

Shi G T, Wang X C, Li Y S, et al. 2019. Organic tracers from biomass burning in snow from the coast to the ice sheet summit of East Antarctica. Atmos Environ, 201: 231-241, doi:10.1016/j.atmosenv. 2018.12.058.

Skiles S M, Painter T H, Deems J S, et al. 2012. Dust radiative forcing in snow of the Upper Colorado River Basin: 2. Interannual variability in radiative forcing and snowmelt rates. Water Resour Res, 48(7): W07522, doi:10.1029/2012wr011986.

Srivastava R, Asutosh A, Sabu, P, et al. 2021. Investigation of black carbon characteristics over Southern Ocean: contribution of fossil fuel and biomass burning. Environ Pollut, 276(D22): 116645, doi:10. 1016/j.envpol.2021.116645.

Vodička P, Schwarz J, Brus D, et al. 2020. Online measurements of very low elemental and organic carbon concentrations in aerosols at a subarctic remote station. Atmos Environ, 226: 117380, doi:10.1016/j. atmosenv.2020.117380.

Wang B, Spessa A C, Feng P Y, et al. 2022. Extreme fire weather is the major driver of severe bushfires in southeast Australia. Sci Bull, 67(6): 655-664, doi:10.1016/j.scib.2021.10.001.

Wang Y T, Bian L G, Ma Y F, et al. 2011. Surface ozone monitoring and background characteristics at Zhongshan Station over Antarctica. Chin Sci Bull, 56(10): 1011-1019, doi:10.1007/s11434-011-4406-2.

Warren S G, Clarke A D. 1990. Soot in the atmosphere and snow surface of Antarctica. J Geophys Res Atmos, 95(D2): 1811-1816, doi:10. 1029/jd095 id02p01811.

Weller R, Minikin A, Petzold A, et al. 2013. Characterization of long-term and seasonal variations of black carbon (BC) concentrations at Neumayer, Antarctica. Atmos Chem Phys, 13(3): 1579-1590, doi:10. 5194/acp-13-1579-2013.

Zhang Y L, Kang S C. 2017. Research progress of light-absorbing impurities in glaciers of the Tibetan Plateau and its surroundings. Chin Sci Bull, 62(35): 4151-4162, doi:10.1360/N972017-00505 (in Chinese with English abstract).

Zhang Y H, Wang Y M, Zhang M M, et al. 2015. Seasonal variations in aerosol compositions at Great Wall Station in Antarctica. Adv Polar Sci, 26: 196-202, doi: 10.13679/j.advps.2015.3.00196.

Zennaro P, Kehrwald N, McConnell J R, et al. 2014. Fire in ice: two millennia of boreal forest fire history from the Greenland NEEM ice core. Clim Past, 10(5): 1905-1924, doi:10.5194/cp-10-1905-2014.

Supplementary Figure
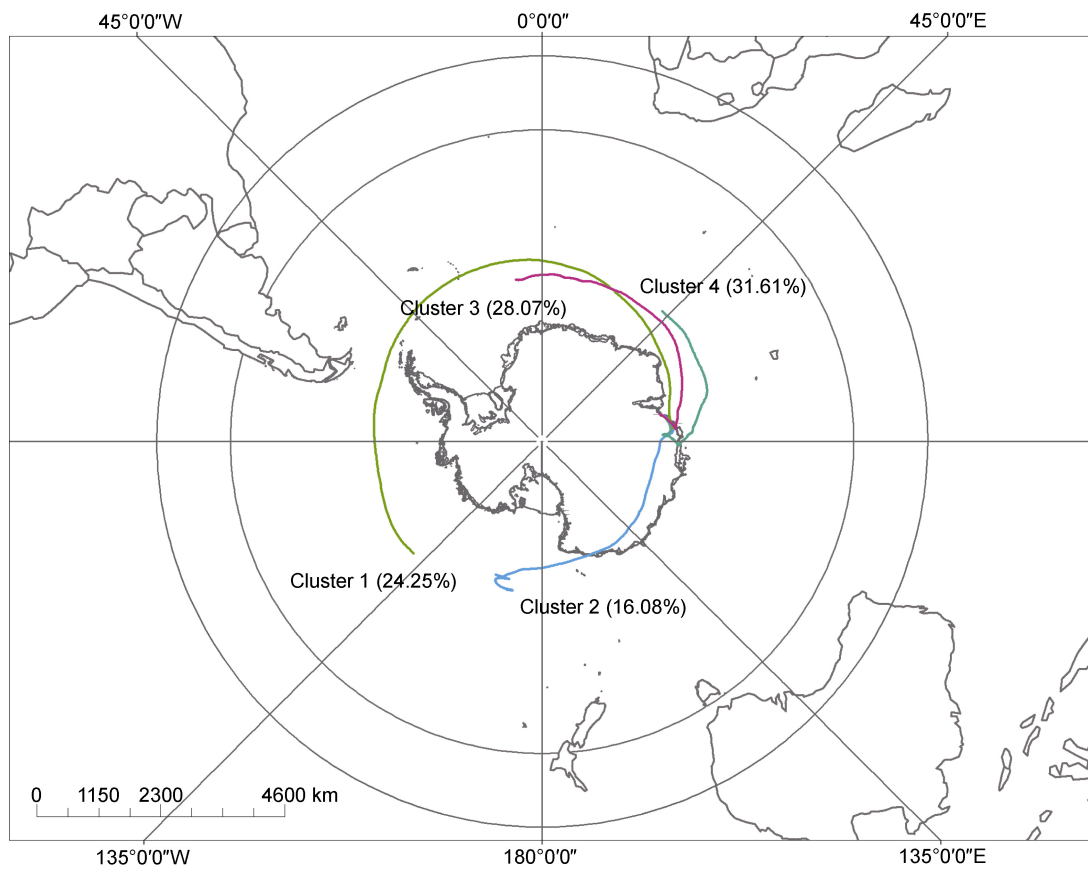
Figure S1   Backward trajectory clustering analysis of 30 d in winter at ZSS from 2017.